ACS POLYMERS Au
AN OPEN ACCESS JOURNAL OF THE AMERICAN CHEMICAL SOCIETY

pubs.acs.org/polymerau

Article

Gaining Structural Control by Modification of Polymerization Rate in Ring-Opening Polymerization-Induced Crystallization-Driven Self-Assembly

Paul Joshua Hurst, Annissa A. Graham, and Joseph P. Patterson*

Cite This: *ACS Polym. Au* 2022, 2, 501−509

Read Online

ACCESS | Metrics & More | Article Recommendations | Supporting Information

ABSTRACT: Polymerization-induced self-assembly (PISA) has become an important one pot method for the preparation of well-defined block copolymer nanoparticles. In PISA, morphology is typically controlled by changing molecular architecture and polymer concentration. However, several computational and experimental studies have suggested that changes in polymerization rate can lead to morphological differences. Here, we demonstrate that catalyst selection can be used to control morphology independent of polymer structure and concentration in ring-opening polymerization-induced crystallization-driven self-assembly (ROPI-CDSA). Slower rates of polymerization give rise to slower rates of self-assembly, resulting in denser lamellae and more 3D structures when compared to faster rates of polymerization. Our explanation for this is that the fast samples transiently exist in a nonequilibrium state as self-assembly starts at a higher solvophobic block length when compared to the slow polymerization. We expect that subsequent examples of rate variation in PISA will allow for greater control over morphological outcome.

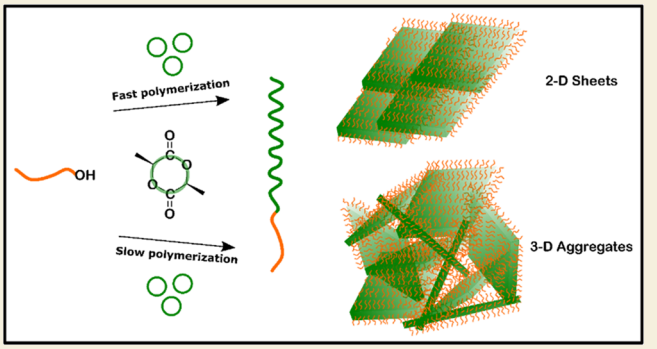

KEYWORDS: *block copolymers, self-assembly, polymerization kinetics, ring-opening polymerization, nonequilibrium, biocompatible polymers*

INTRODUCTION

Polymerization-induced self-assembly (PISA) has revolutionized the synthesis of block copolymer self-assemblies as it enables the reproducible scaled-up production of nanoparticles.[1−4] Compared to traditional self-assembly, which generally yields solutions that are 1% solids w/w, PISA can garner solutions ranging from 10 to 50% solids w/w and enables easy access to a range of higher-ordered morphologies such as worms and vesicles.[4,5] PISA has been developed for a wide range of polymerization techniques[4,6−12] with the most studied method being reversible addition−fragmentation chain-transfer (RAFT).[4,6,7] In addition, PISA for crystalline and semicrystalline polymers, termed polymerization-induced crystallization-driven self-assembly (PI-CDSA), has been developed allowing for the scaled-up production of anisotropic nanostructures such as rods and lamellae.[13−18]

Recently, we developed PISA for the ring-opening polymerization (ROP) of semicrystalline polyesters, termed ring-opening polymerization-induced crystallization-driven self-assembly (ROPI-CDSA).[15] This process occurred by chain extending polyethylene glycol (PEG) with L-lactide in toluene using triazabicyclodecene (TBD) as the catalyst. The resulting poly(L)-lactide-*block*-polyethylene glycol (PLLA-*b*-PEG) particle morphology could be controlled by changing the polymer structure (degree of polymerization (DP)) and concentration, as is common with other PISA processes.[2,7] In contrast to most PISA examples where self-assembly is fast with respect to polymerization,[19] there was a delay between the polymerization and self-assembly. TBD-catalyzed ROP of L-lactide is very fast (∼1 min), whereas the resulting self-assembly, which was driven by crystallization, was considerably slower (∼hours). Due to this delay, we could trap different morphologies post-polymerization by freeze-drying and redispersing the samples in water where the structures become kinetically trapped. This trapping enables time post-polymerization to be an additional factor to control morphology in PISA experiments. This strategy is advantageous as it enables different morphologies to be formed from the same polymer and at the same concentration. Our interpretation of this data was that, during the polymerization, the polymers are in a

Received: June 16, 2022
Revised: August 17, 2022
Accepted: August 18, 2022
Published: August 26, 2022

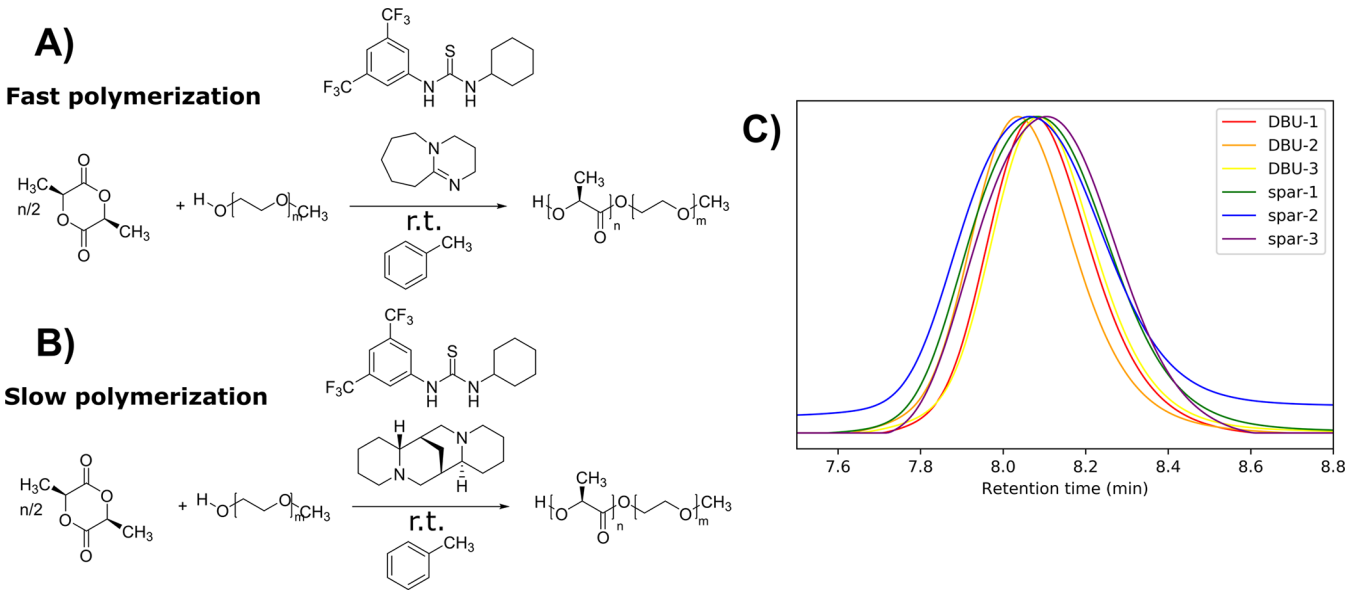

Figure 1. Polymerization schemes and SEC data. ROP of L-lactide to produce PLLA-*b*-PEG catalyzed by TU and (A) DBU or (B) (−)-sparteine. (C) Triplicate SEC data for $PLLA_{200}$-*b*-PEG_{45} for polymers **1**−**3** and **7**−**9**. All $Đ \approx 1.1$ indicating a controlled polymerization.

nonequilibrium state as the chains are temporarily soluble in the selective solvent. Thus, we hypothesize that a modification in the polymerization kinetics would lead to a change in the nonequilibrium state, resulting in a different self-assembly mechanism, allowing access to different morphologies.

Dissipative particle dynamics (DPD) simulations have indicated that polymerization rate can be used to control morphology of poly(4-vinylpyridine)-*b*-polystyrene PISA processes.[20,21] The explanation for the change in morphology was that fast polymerization rates led to larger amounts of exposed solvophobic block resulting in a faster rate of self-assembly. Experimentally, photoinitiated vs thermally initiated processes, changes in initiator concentration, solvent composition, monomer types, and Z-group substitution, in the case of RAFT-PISA, have shown differences in morphology, which have been attributed to changes in the rate of polymerization.[6,9,17,22−25] However, there is limited quantitative information on how the rate of polymerization affects morphology because designing experiments to modulate the propagation rate constant, k_p, without affecting thermodynamic parameters or polymerization control is difficult. For example, changing monomer type, temperature, or solvent composition will also change the free energy landscape for the assembly process making it difficult to assign differences in morphology to kinetic effects alone. Additionally, the relaxation time is typically fast for RAFT-PISA processes, limiting mechanistic studies into potential nonequilibrium states.

Generally, in controlled polymerization, k_p depends on the nature of the monomer under a given temperature and solvent; however, the presence of a catalyst can modulate k_p without changing the environment. In the ROP of polyesters, a variety of catalytic systems have been developed, allowing for the polymerization of one monomer with a range of k_p values.[26,27] Thus, we can use different catalysts in ROPI-CDSA to monitor polymerization kinetics and compare any differences between the resulting self-assemblies.

Here, to test our hypothesis, we report the use of two ROP catalytic systems (one fast and one slow) to alter the polymerization rate of L-lactide and the self-assembly of PLLA-*b*-PEG block copolymers. Kinetic studies of polymerization and self-assembly were conducted using ^{1}H NMR and UV/vis spectroscopy, respectively. Rheology was used to probe the mechanical properties of the resulting organogels. Wide-angle X-ray scattering (WAXS), and Fourier-transform infrared spectroscopy (FTIR) were used to determine crystallization properties. Dry cryogenic-transmission electron microscopy (cryo-TEM), scanning electron microscopy (SEM), and atomic force microscopy (AFM) were used to determine the nanoscale morphology.

RESULTS

Testing the hypothesis that polymerization kinetics affects the morphology of ROPI-CDSA reactions requires two systems with almost identical thermodynamics and significantly different kinetics (fast or slow). Therefore, all ROPI-CDSA reactions were performed in the same solvent (toluene), at the same temperature and concentration, forming PLLA-*b*-PEG block copolymers with the same molecular weight and dispersity. The polymerization kinetics were controlled by catalyst selection. TBD was not used as a catalyst due to reports of potential transesterification at higher degrees of polymerization.[15,28] Hedrick and Waymouth et al.[29,30] developed a dual catalytic system for the polymerization of cyclic esters which utilizes a thiourea (TU), derived from cyclohexylamine and 3,5-bis(trifluoromethyl)phenyl isothiocyanate, paired with a tertiary amine or diazabicycloundecene (DBU). The amidine DBU (1% mol) was paired with TU (7.5% mol) for the fast reaction and the tertiary amine (−)-sparteine (7.5% mol) was paired with TU (7.5% mol) for the slow reaction (Figure 1A,B). DBU can catalyze the ROP of L-lactide without TU due to its higher basicity, but to control environmental conditions, 7.5% mol TU was used in both the slow and fast reactions. A series of fast and slow polymerizations were carried out, varying PLLA DP (200, 400) and solids content (10, 15, 20 w/w%). The PLLA DP 200, 10% systems were repeated three times for reproducibility.

The resulting polymers were analyzed by size exclusion chromatography (SEC) and ^{1}H NMR spectroscopy. Both

https://doi.org/10.1021/acspolymersau.2c00027
ACS Polym. Au 2022, 2, 501−509

catalytic systems reached >95% conversion with $Đ$ < 1.2, indicating a controlled polymerization (Figure 1C, Table 1, Table S1, Figures S1–S3). The polymerization kinetics of PLLA DP = 200, 10% solids w/w, reactions (**1**–**3**, **7**–**9**) were studied using ^{1}H NMR spectroscopy. The rate equation for a dicatalytic ROP system depends on the concentration of both active catalytic species (TU and cocat), the initiator (I), and the monomer (LA) (eq 1).[30]

$$-\frac{\mathrm{d[LA]}}{\mathrm{d}t} = -k_p K_1 K_2 [\mathrm{TU}][\mathrm{cocat}][\mathrm{I}][\mathrm{LA}] = -k_{app}[\mathrm{LA}] \quad (1)$$

As only the monomer concentration changes, the system can be modeled as a pseudo-first order reaction. Because finding the propagation rate constant (k_p) would require thermodynamic knowledge of the catalyst-monomer association constants,[30] the apparent propagation rate constant (k_{app}) was found. ^{1}H NMR kinetic studies show two k_{app} values for both polymerization processes (1st k_{app}: fast k_{app} = 19 ± 2 h^{-1}, slow k_{app} = 0.16 ± 0.02 h^{-1}) with an increase in k_{app} that corresponds to the onset of turbidity of the self-assembly (2nd k_{app}: fast k_{app} = 40 ± 3 h^{-1}, slow k_{app} = 0.54 ± 0.12 h^{-1}) (Figure 2, Table 2, Figures S4 and S5) consistent with previous PISA literature.[2,22,31,32] There is a 3-fold increase in k_{app} for the slow polymerization compared to a 2-fold increase for the fast polymerization. Increases in the propagation rate are usually explained by a high local concentration of monomer in or near the self-assembled phase. Differences in the local environment or growth mechanism could explain the difference in the percent increase of k_{app} although further research would be needed to verify this. The self-assembly kinetics were probed using UV/vis spectroscopy performed at 600 nm to measure turbidity (Figures 2, S6, and 7). The turbidity studies confirm that self-assembly starts at approximately the same time as the change in k_{app}, indicating that the onset of self-assembly increases k_{app}. The (−)-sparteine cocatalyzed slow polymerization system became turbid around 70% (PLLA DP = 140) conversion compared to 85% conversion (PLLA DP = 170) for the fast DBU cocatalyzed polymerization system. Additionally, the time to maximum turbidity is substantially different for the fast polymerization and slow polymerization samples taking ∼0.15 and 12 h, respectively. The turbidity data appears to be sigmoidal, which has been observed in a variety of self-assembly processes.[33−36] Therefore, the data was modeled as a logistic function (eq 2).

$$f(x) = \frac{L}{1 + e^{-k(x-x_0)}} + m \quad (2)$$

where L is the maximum value of the function, m is the intercept, x_0 is the x value of the steepness point of the curve, and k quantifies the steepness of the sigmodal curve. Here k can then be used as a numerical quantification of the rate of turbidity, which is an estimate for the rate of self-assembly. Fitting the data to the logistic function gives $k_{turbidity}$ of 70.2 and 0.98 h^{-1} for the fast and slow polymerization systems, respectively. Thus, both the rate of polymerization (k_{app}) and

Table 1. Polymerization Table of PLLA$_n$-*b*-PEG$_{45}$ Block Copolymers Synthesized in This Study

ID	cocatalyst	PLLA DP	solids w/w%	$Đ$	gel (Y/N)
1	DBU	200	10	1.06	N
2	DBU	200	10	1.16	N
3	DBU	200	10	1.12	N
4	DBU	200	15	1.14	N
5	DBU	200	20	1.17	Y
6	DBU	400	10	1.14	N
7	(−)-sparteine	200	10	1.16	Y
8	(−)-sparteine	200	10	1.10	Y
9	(−)-sparteine	200	10	1.17	Y
10	(−)-sparteine	200	15	1.16	Y
11	(−)-sparteine	200	20	1.13	Y
12	(−)-sparteine	400	10	1.15	Y

Table 2. Polymerization Kinetics Studies of PLLA$_{200}$-*b*-PEG$_{45}$[a]

ID	cocatalyst	1st k_{app} h^{-1}	2nd k_{app} h^{-1}
1	DBU	17	42
2	DBU	18	40
3	DBU	21	37
avg	DBU	19 ± 2	40 ± 3
7	(−)-sparteine	0.18	0.60
8	(−)-sparteine	0.17	0.63
9	(−)-sparteine	0.13	0.40
avg	(−)-sparteine	0.16 ± 0.02	0.54 ± 0.12

[a]All trendlines used had R^2 > 0.95.

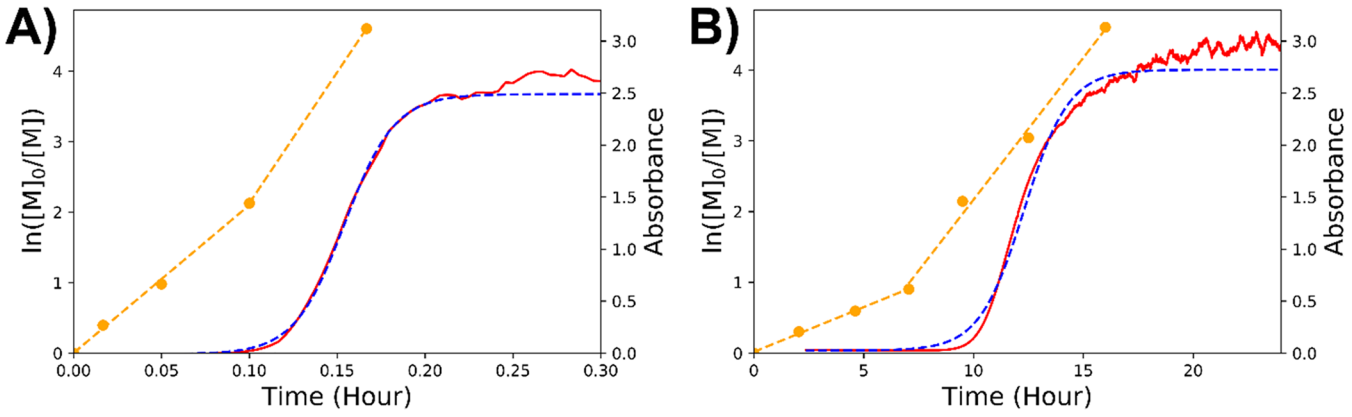

Figure 2. Polymerization and self-assembly kinetics for the (A) fast and (B) slow polymerizations of PLLA$_{200}$-*b*-PEG$_{45}$. The orange markers are the measured values of ln[M]$_0$/[M] with the dotted line representing the linear fit. The red line is the measured absorbance at 600 nm using UV/vis spectroscopy with the blue line being the logistic fit.

https://doi.org/10.1021/acspolymersau.2c00027
ACS Polym. Au 2022, 2, 501−509

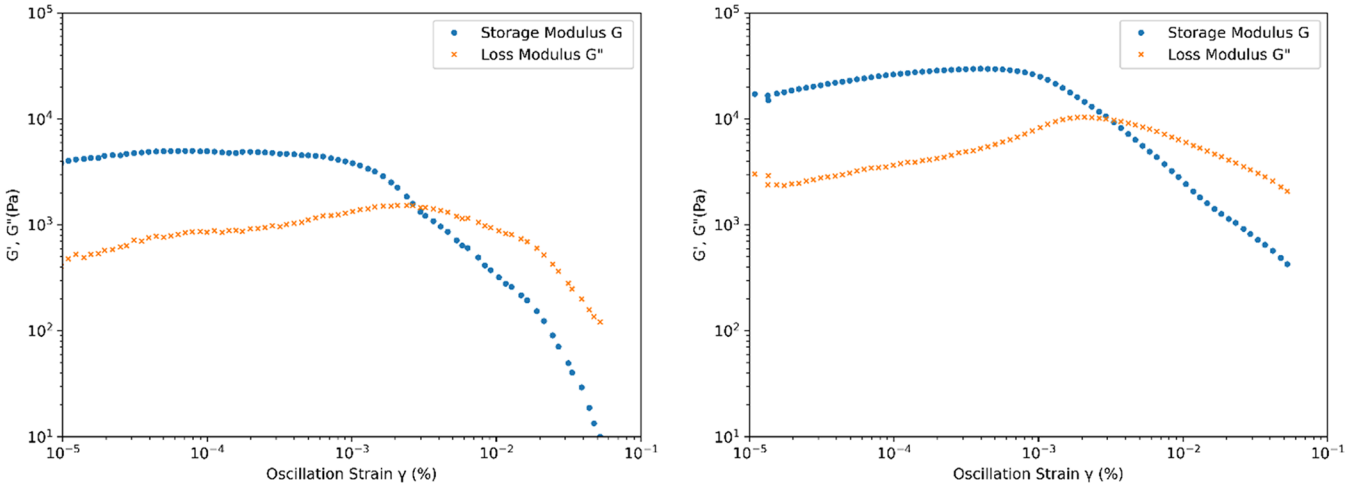

Figure 3. Oscillatory rheology for organogels **5** (left, DBU cocatalyst) and **11** (right, (−)-sparteine cocatalyst) for $PLLA_{200}$-*b*-PEG_{45} at 20% solids w/w. **11** has a storage modulus nearly 1 order of magnitude higher than that of **5**, indicating it is the stronger gel.

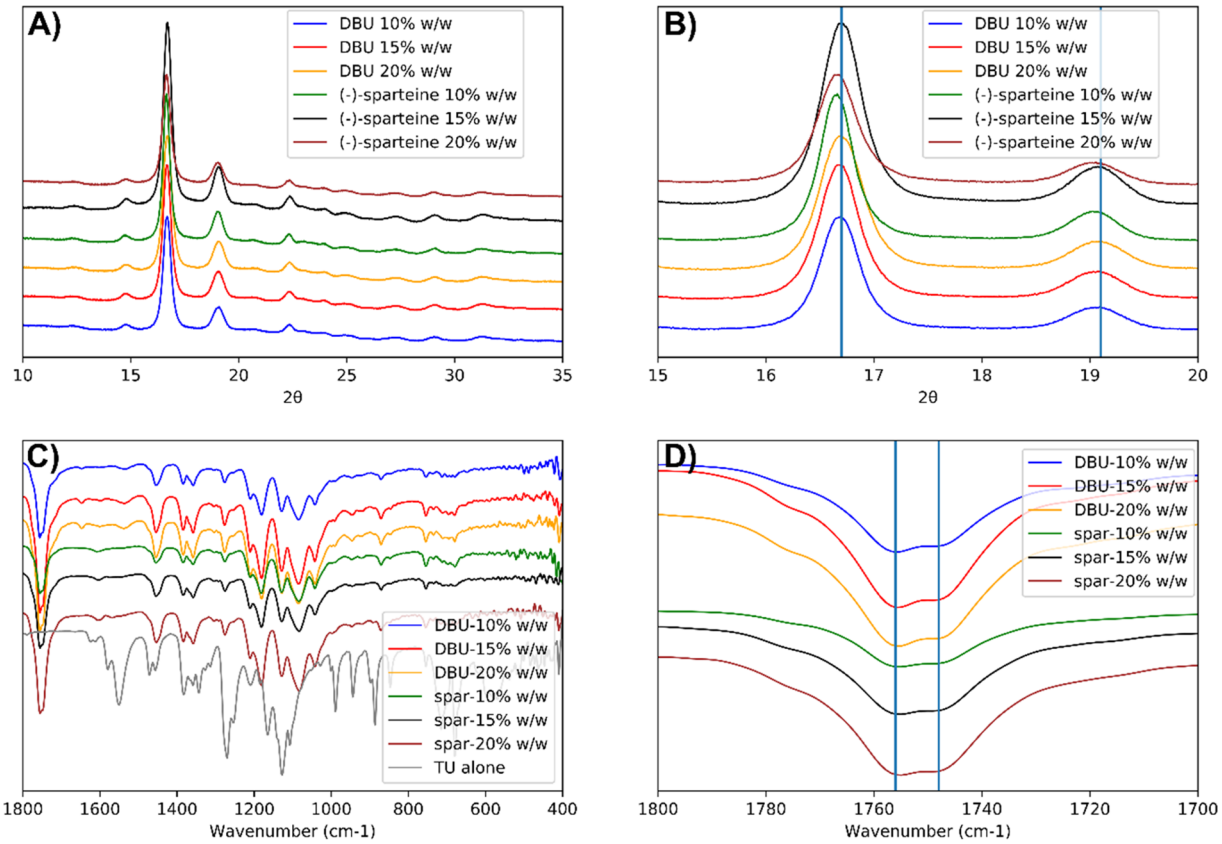

Figure 4. WAXS patterns and FTIR spectra for $PLLA_{200}$-*b*-PEG_{45} freeze-dried samples. (A) WAXS overview. (B) Close up on the two major peaks reveal slight offsets between the (−)-sparteine and DBU cocatalyzed samples. (C) FTIR spectra of fingerprint and carbonyl region. (D) FTIR of carbonyl with lines at 1748 and 1756 cm^{-1}.

the rate of self-assembly ($k_{turbidity}$) are much greater in the fast polymerization than in the slow polymerization.

In addition to the variable polymerization and self-assembly kinetics, structural and morphological differences were observed between the fast and slow polymerization samples. The slow polymerizations, cocatalyzed by (−)-sparteine (**7**−**12**), led to the formation of organogels as defined by a gel-inversion test and oscillatory rheology (Figures 3 and S8). Only sample **5** for the fast reactions, cocatalyzed by DBU, formed a gel while the rest of the samples remained liquid (Figure 3). At 20% solids w/w, the storage modulus of the slow polymerization sample, **11**, was about an order of magnitude higher (10^4) than that of the fast polymerization sample (10^3), **5**. As a control experiment, to determine if cocatalyst differences were responsible for the rheological differences, polymerizations were carried out using (−)-sparteine or DBU ($PLLA_{200}$-*b*-PEG_{45}, 10% solids w/w), and upon quenching with benzoic acid, the other cocatalyst was added (DBU to (−)-sparteine polymerized solutions and (−)-sparteine to DBU polymerized solutions). No appreciable

https://doi.org/10.1021/acspolymersau.2c00027
ACS Polym. Au 2022, 2, 501−509

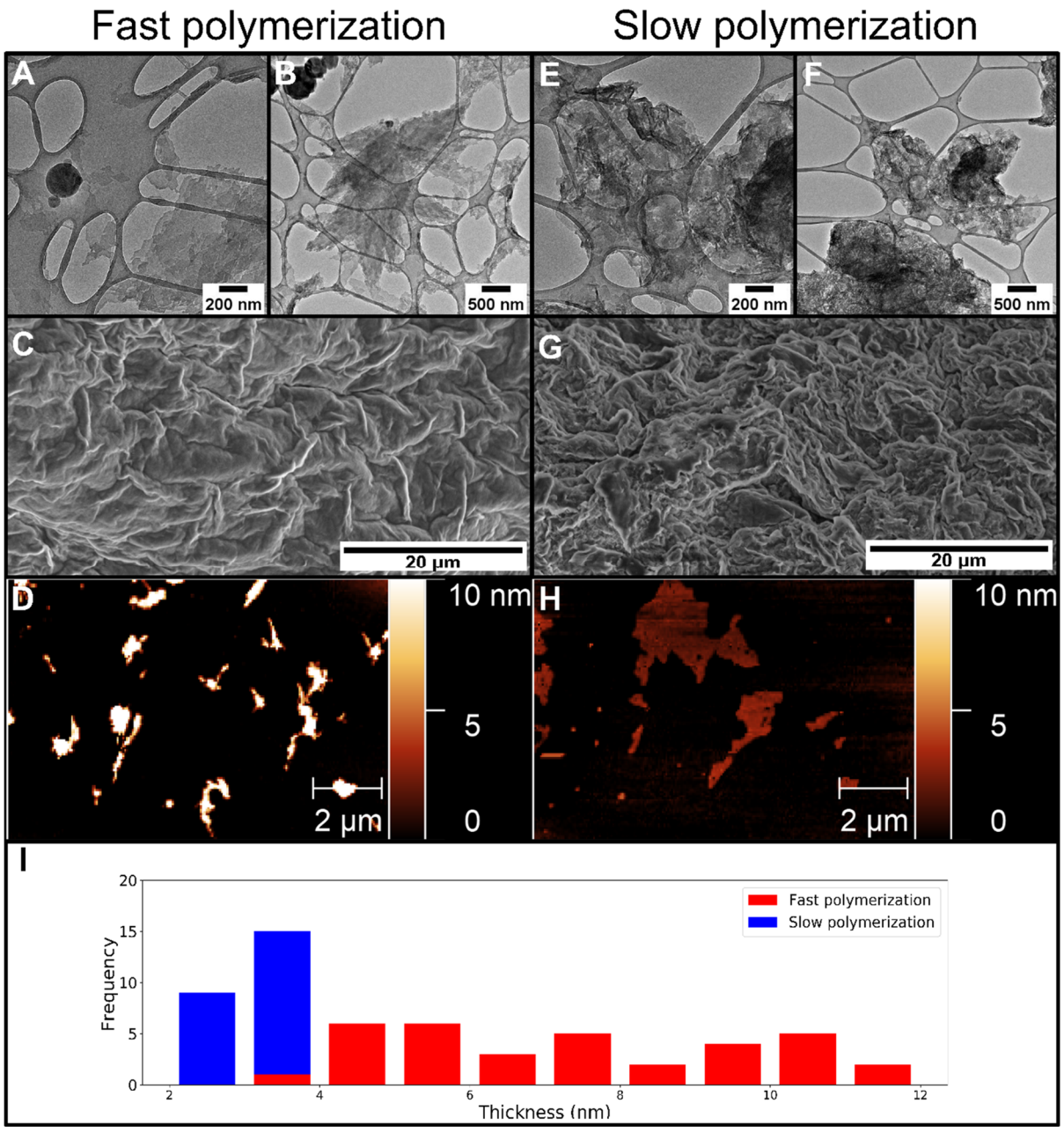

Figure 5. Dry cryo-TEM, SEM, and AFM micrographs and histogram of $PLLA_{200}$-*b*-PEG_{45} assemblies resulting from a fast polymerization with cocatalyst DBU (A–D) and slow polymerization with with-cocatalyst (−)-sparteine (E–H). The stacked histogram (I) shows measurements for the fast polymerization in red and the slow polymerization in blue. The slow polymerization yields denser structures as shown in (E)−(G), but the individual lamellae are thinner (H–I) than the fast polymerization structures (D, I).

differences in the storage modulus were detected by oscillatory rheology in organogel samples between the control and the noncontrol for the slow polymerization samples (Figure S8). Both fast polymerization samples remained liquids. This indicates that the differences between the fast and slow polymerizations are not related to the different cocatalysts, but are due to the differences in polymerization rate.

WAXS and FTIR were then performed on freeze-dried powders of **1**−**12** to elucidate if structural differences were a result of differences in crystallization behavior (Figures 4 and S9). WAXS shows that the crystallinity between the catalytic groups is very similar (Figure 4A,B). The calculated % crystallinity ranges for all samples are around 23%, indicating that both systems crystallized to a similar extent (Table S2). WAXS data show no evidence of TU crystallization suggesting that the TU is well integrated into the polymer matrix (Figure S10). At 2θ 16.7 and 19.1, there are some small differences in peak positions (<0.03); however, triplicate runs of **7**−**9** show that peak values between the same sample have a standard deviation of 0.03 (Figure S11), indicating these differences are statistically insignificant. FTIR shows that the carbonyl environment is similar in all samples and suggests supramolecular interactions between the TU and the PLLA ester (Figure 4C,D). In this work, the PLLA C═O stretches have two peaks at 1748 and 1756 cm^{-1} (Figure 4D). In the first example of ROPI-CDSA, the C═O shifts were 1749 and 1754 cm^{-1}, indicating differences in the carbonyl environment from the exclusion of TU.[15] Furthermore, a lack of N−H stretches is

https://doi.org/10.1021/acspolymersau.2c00027
ACS Polym. Au 2022, 2, 501−509

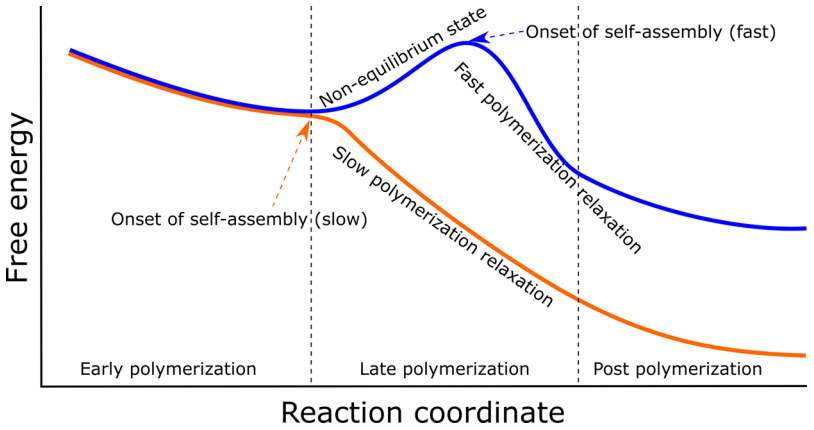

Figure 6. Free energy diagram of ROPI-CDSA resulting from fast polymerization (blue) and slow polymerization (orange). The polymerization is divided into three stages: Early polymerization where the polymers do not have a thermodynamic driving force to assemble, late polymerizations where the polymers have a thermodynamic driving force to assembly, and post-polymerizations. Due to the relative rates of polymerization and self-assembly, the fast polymerization temporarily accesses a nonequilibrium state leading to differences in the final kinetically trapped morphology.

an indication that the N−H groups in the TU are hydrogen bonding with C═O (Figure S12).[37] Moreover, other TU stretches are offset from their original values indicating that the TU is well integrated into the polymer structure (Figure 4C).

To determine the structure of the resulting self-assemblies and organogels, dry cryo-TEM, SEM, and AFM were performed on **1** and **7** (Figure 5). In contrast to our previous study,[15] the polymer toluene solutions could not be resuspended or extracted into water without precipitation. This is likely due to the hydrophobicity of the TU which is incorporated into the block copolymer self-assemblies. Therefore, a dry sample was imaged under cryogenic conditions (dry cryo-TEM) to minimize beam damage to the sample.[38] Cryo-TEM images of the fast polymerization sample, **1**, revealed planar 2D aggregates (Figures 5A,B and S13), whereas the slow polymerization sample, **7**, revealed complex 3D aggregates (Figure 5E,F). AFM revealed that the lamellae thickness of **1**, the fast polymerization sample, was significantly thicker (Figure 5D,I, 5.6 ± 1.2 nm, n = 21) than that of **7**, the slow polymerization sample (Figure 5H,I, 3.0 ± 0.2 nm, n = 23). These values are thin compared to our previous paper and other relevant examples of PLLA-based block copolymer assemblies, and further work is needed to understand the exact folding.[15,39,40] It should also be noted that the fast polymerization sample AFM micrograph showed the presence of double-stacked lamellae (10.2 ± 1.1 nm, n = 14) as well as higher ordered stacks, whereas the slow polymerization only showed single lamellae (Figures S14 and S15). Due to the fact that the PEG block will contribute to this measurement, it is not possible to determine the folding factor for the PLLA block.[15] However, considering that both samples have the same molecular structure and assuming that drying artifacts are similar, this indicates that the PLLA blocks in the fast reaction are significantly less folded than those in in the slow reaction. This lower degree of folding can explain why 2D aggregates are favored over 3D aggregates.

DISCUSSION

The combined SEC, ^{1}H NMR, WAXS, and FTIR data reveal that the PLLA$_{200}$-*b*-PEG$_{45}$, polymers have the same molecular structure and crystallization behavior regardless of cocatalyst. Despite these similarities, the rheology, cryo-TEM, SEM, and AFM data reveal that the fast and slow reactions form different structures in solution. The fast reactions favor the formation of 2D lamellae, resulting in solutions or weak gels, whereas the slow reactions favor the formation of 3D networks and stronger gels. The ^{1}H NMR and turbidity kinetics studies show that the slow reactions become turbid at lower conversions and have a slower rate of self-assembly. Our previous paper studied the mechanism of ROPI-CDSA and revealed that the 3D networks can form through a particle aggregation-based mechanism.[15] We hypothesized that this was facilitated by forming structures with a low corona density as this would lower the energy barrier to aggregation.[41] The data here is consistent with this hypothesis as the AFM lamellae thickness measurements show that the PLLA blocks in the slow reactions are much more folded than those in the fast reactions. Given that both the fast and slow reactions form polymers with the same degree of polymerization, this would result in the assemblies in the slow reactions having lower corona densities that favor aggregation and the formation of 3D networks.

In our previous paper, the polymerization time was much shorter (seconds to minutes) than the self-assembly relaxation time (hours to days). From a thermodynamic perspective, we interpreted this as forming a nonequilibrium state as the system does not have sufficient time to relax with each monomer addition. Here, the polymerization is sufficiently slow such that self-assembly begins before polymerization is complete. The fast DBU-catalyzed polymerization becomes turbid at higher conversions compared to the slow (−)-sparteine-catalyzed polymerization. In discussing the relative free energy of these two systems, we can divide the free energy diagram into three stages: early polymerization, late polymerization, and post-polymerization (Figure 6). In the early polymerization stage, the polymer chains are not sufficiently solvophobic to assemble or crystallize and consequently the free energy decreases as the polymerization progresses for both the fast and slow polymerizations. In the late polymerization state, the polymer chains are sufficiently solvophobic to initiate self-assembly and crystallization. For the slow reaction, the free energy continues to decrease because the chains are able to undergo self-assembly and crystallization. For the fast reaction, the polymer chains do not undergo assembly or crystallization and, therefore, transiently exist in a nonequilibrium state until the onset of self-assembly. When the fast polymerization system begins to self-assemble, it does so

https://doi.org/10.1021/acspolymersau.2c00027
ACS Polym. Au 2022, 2, 501−509

with a greater exposed surface-area of solvophobic PLLA blocks, leading to enhanced self-assembly kinetics and more aggregation. A consequence of this is that the fast polymerization system becomes kinetically trapped at a higher free energy relative to the slow polymerization system. Lastly, in the post-polymerization stage, additional relaxation for both systems is observed, highlighting a lag in self-assembly kinetics with respect to polymerization.

CONCLUSION

In conclusion, we have demonstrated that polymerization rate has a significant effect on the self-assembly rate, morphological outcome, and structural properties in the ROPI-CDSA of PLLA-*b*-PEG block copolymers. In this specific case, slow polymerizations result in more folded PLLA chains, earlier stage self-assembly, slower self-assembly kinetics, and the formation of 3D networks. In contrast, fast polymerizations results in less folded PLLA blocks, later stage self-assembly, faster self-assembly kinetics, and 2D structures. The differences in morphology are attributed to differences in the assembly mechanism, which is driven by nonequilibrium chemistry in the fast reaction. Therefore, in addition to the variables of polymer architecture, solution concentration, and time post-polymerization, changing the rate of polymerization can be used to control polymer morphology. Thus, we can use the rate of polymerization to gain structural control without the modification of molecular structure. As additional polymerization methods and catalysts are developed, we anticipate that polymerization rate will be commonly used to manipulate morphology. Furthermore, we anticipate that the phenomena described here is applicable to all PISA processes if the relative rates of polymerization and self-assembly can be appropriately controlled.

EXPERIMENTAL SECTION

Materials

mPEG45 (MW = 2000) (Sigma-Aldrich) was azeotropically distilled ×2 in toluene and high-vacuumed overnight. L-Lactide (TCI) was recrystallized in toluene ×3. Anhydrous toluene (99.8%), DBU, and (−)-sparteine were obtained from Sigma-Aldrich and stored under 4 Å molecular sieves. Benzoic acid (Fisher Chemical) was used without further purification. Thiourea (TU) derived from cyclohexylamine (Sigma-Aldrich) and 3,5-bis(trifluoromethyl)phenyl isothiocyanate (TCI) was synthesized following established literature procedures.[29] Chemicals were stored in a dry-N_2 atmosphere glovebox. Reactions were performed in a N_2 glovebox.

DBU and TU Catalyzed (Fast Polymerization) PLLA-*b*-PEG Synthesis and Self-Assembly

Procedure adapted from Hedrick and Waymouth et al.[29,30] L-Lactide (288 mg, 2 mmol, PLLA target DP = 200) was added to a solution of mPEG45 (40 mg, 20 μmol) and 7.5% mol TU (51 mg, 150 μmol) in 4.0 mL of toluene (10% solids w/w). Next, 1% mol DBU (3 μL, 30 μmol) was added. The solution was stirred for 16 m and subsequently quenched with 0.05 mL of saturated benzoic acid toluene solution. Stirring was kept at 400 rpm for reproducibility, and solutions were stirred for at least 24 h post-polymerization. ^{1}H NMR (500 MHz, CDCl3) δ 5.16 (q, J = 7.0 Hz, CH, PLLA backbone), 3.72−3.59 (m, CH2 PEG backbone), 3.54 (dd, J = 5.6, 3.6 Hz, CH2, PEG), 3.37 (s, 3H, terminal CH3 PEG), 1.58 (d, J = 6.7 Hz, CH3 PLLA backbone), 1.50 (dd, J = 14.7, 7.0 Hz, terminal CH3 PLLA).

(−)-Sparteine and TU Catalyzed (Slow Polymerization) PLLA-*b*-PEG Synthesis and Self-Assembly

Procedure adapted from Hedrick and Waymouth et al.[29] L-Lactide (288 mg, 2 mmol, PLLA target DP = 200) was added to a solution of mPEG45 (60 mg, 30 μmol) and 7.5% mol TU (51 mg, 150 μmol) in 4.3 mL of toluene (10% solids w/w). Next, 7.5% mol (−)-sparteine (35 μL, 150 μmol) was added. The solution was stirred for 24 h and subsequently quenched with 0.05 mL of saturated benzoic acid toluene solution. Stirring was kept at 400 rpm for reproducibility, and solutions were stirred for at least 24 h post-polymerization. ^{1}H NMR (500 MHz, CDCl3) δ 5.16 (q, J = 7.0 Hz, CH, PLLA backbone), 3.72−3.59 (m, CH2 PEG backbone), 3.54 (dd, J = 5.6, 3.6 Hz, CH2, PEG), 3.37 (s, 3H, terminal CH3 PEG), 1.58 (d, J = 6.7 Hz, CH3 PLLA backbone), 1.50 (dd, J = 14.7, 7.0 Hz, terminal CH3 PLLA).

Lyophilization

Lyophilized powders were obtained by freezing the toluene solutions in a round-bottom flask with liquid nitrogen followed by sublimation using a vacuum pump.

Structural Characterization and Polymerization Kinetics

Proton nuclear magnetic resonance (^{1}H NMR) spectra were collected on a 500 MHz Bruker Avance spectrometer in $CDCl_3$. Chemical shifts are given in ppm, calibrated from residual $CHCl_3$. Polymerization kinetics were collected by dropping 0.1 mL of reaction mixture into a vial with a drop of saturated benzoic acid solution and diluting in $CDCl_3$. Conversion was calculated from comparing the peak area of the PLLA peak at 5.16 to the L-lactide monomer peak at 5.03.[15] Size exclusion chromatography (SEC) was performed in THF using an Agilent 1100 chromatograph equipped with RID detector and a PL gel 5 μm 300 × 7.5 mm mixed column. Samples were calibrated against polystyrene standards.

Turbidity Measurements

Self-assembly kinetics were measured on an Agilent Technologies Cary 60 UV−vis spectrometer in a N_2 atmosphere in a glovebox using a 1 cm path length quartz cuvette. Changes in turbidity were measured at 600 nm every 15 s until the measurement plateaued with a moderate stirring rate.

Rheology

Oscillatory rheology was collected from organogels on a TA DHR 2 rheometer. Gels were loaded using a 20 mm steel Peltier plate. Measurements were taken from 1.0×10^{-3} to 100.0 strain % at 25 °C.

Crystallinity Characterization

Wide-angle X-ray scattering (WAXS) patterns were measured on a Rigaku Smart lab X-ray diffractometer in Bragg−Brentano diffraction mode utilizing X-rays generated at 40 kV and 44 mA with Cu Kα irradiation (step size 0.02°, speed 1.0, IS 0.5°, RS1 4.0°, RS2 13 mm). Approximately 20 mg of a lyophilized sample was used in measurements. Crystallinity was estimated using the Smart lab software after peaks were assigned to PLLA-*b*-PEG. Fourier transform infrared (FTIR) absorbance spectra were collected on a Jasco 4700 FTIR from lyophilized samples.

Morphological Characterization

Dry cryogenic-transmission electron microscopy (cryo-TEM) samples were prepared from toluene samples that were freshly diluted ×100 onto Lacey Carbon (Electron Microscopy Sciences) grids. Vitrification was carried out by an Automatic Plunge Freezer ME GP2 (Leica Microsystems) with 3 μL of sample. Grid preparation was performed at ambient humidity and the grids were blotted for 3 s prior to plunging into liquid nitrogen. Cryo-TEM samples were then placed on a Gatan cryo-TEM holder and imaged on a JEOL 2100F transmission electron microscope using a Schottky type field emission gun operating at 200 keV. Images were recorded using SerialEM software in low dose imaging mode with a Gatan OneView CMOS camera at 4k × 4k resolution.

Scanning electron microscopy (SEM) samples were prepared from lyophilized samples which were freeze-cracked in liquid N2 and coated ex situ with 3 nm of iridium (Quorum, Q150T Plus). Secondary electron images were collected on a FEI Magellan 400 scanning electron microscope, Quanta 3D FEG with Everhart-Thornley detector, using a 5 kV acceleration potential, and a probe current of 200 pA.

https://doi.org/10.1021/acspolymersau.2c00027
ACS Polym. Au 2022, 2, 501−509

Atomic force microscopy (AFM) micrographs were collected on a Anton Paar atomic force microscope in tapping mode using Arrow silicon noncontact tapping mode reflex coating tips (Nanoworld). Samples were drop-casted from toluene samples that were freshly diluted by ×100 on silicon nitride chips. Micrographs were processed using Gwyddion. The images were leveled by mean plane subtraction, and rows were aligned using matching. The polynomial background was removed (degree = 3), and horizontal scars were corrected. The lower and upper percentiles in each image were limited by 0.2% to remove noise artifacts.

■ ASSOCIATED CONTENT

Supporting Information

The Supporting Information is available free of charge at https://pubs.acs.org/doi/10.1021/acspolymersau.2c00027.

Tables of polymer characterization data and crystallinity. Figures of SEC traces, polymerization and turbidity kinetics, oscillatory rheology, WAXS, FTIR, additional cryo-TEM, AFM images and measurement histograms (PDF)

■ AUTHOR INFORMATION

Corresponding Author

Joseph P. Patterson − *Department of Chemistry, University of California, Irvine, Irvine, California 92697-2025, United States; Department of Materials Science and Engineering, University of California, Irvine, Irvine, California 92697-2025, United States;* orcid.org/0000-0002-1975-1854; Email: patters3@uci.edu

Authors

Paul Joshua Hurst − *Department of Chemistry, University of California, Irvine, Irvine, California 92697-2025, United States;* orcid.org/0000-0002-1826-2549

Annissa A. Graham − *Department of Chemistry, University of California, Irvine, Irvine, California 92697-2025, United States*

Complete contact information is available at: https://pubs.acs.org/10.1021/acspolymersau.2c00027

Author Contributions

CRediT: **Paul Joshua Hurst** conceptualization (supporting), data curation (lead), formal analysis (equal), investigation (equal), methodology (equal), writing-original draft (equal), writing-review & editing (equal); **Annissa A Graham** data curation (supporting), formal analysis (supporting), investigation (supporting), methodology (supporting), writing-review & editing (supporting); **Joseph P. Patterson** conceptualization (lead), funding acquisition (lead), supervision (lead), writing-original draft (equal), writing-review & editing (equal).

Notes

The authors declare no competing financial interest.

■ ACKNOWLEDGMENTS

This research was partially supported by the National Science Foundation Materials Research Science and Engineering Center program through the UC Irvine Center for Complex and Active Materials (DMR-2011967). IMRI (CTEM, TEMPR, LEXI) Linear lab (FTIR). The authors acknowledge the use of facilities and instrumentation at the UC Irvine Materials Research Institute (IMRI), which is supported in part by the National Science Foundation through the UC Irvine Materials Research Science and Engineering Center (DMR-2011967) as well as the UCI laser spectroscopy lab (https://www.chem.uci.edu/~dmitryf/index.html). The authors would also like to thank their colleagues in the Guan lab for the use of their SEC instrumentation and the Yang lab for the use of their air free UV/vis instrumentation.

■ REFERENCES

(1) Charleux, B.; Delaittre, G.; Rieger, J.; D'Agosto, F. Polymerization-Induced Self-Assembly: From Soluble Macromolecules to Block Copolymer Nano-Objects in One Step. *Macromolecules* **2012**, *45* (17), 6753−6765.

(2) Canning, S. L.; Smith, G. N.; Armes, S. P. A Critical Appraisal of RAFT-Mediated Polymerization-Induced Self-Assembly. *Macromolecules* **2016**, *49* (6), 1985−2001.

(3) Penfold, N. J. W.; Yeow, J.; Boyer, C.; Armes, S. P. Emerging Trends in Polymerization-Induced Self-Assembly. *ACS Macro Lett.* **2019**, *8* (8), 1029−1054.

(4) Yeow, J.; Boyer, C. Photoinitiated Polymerization-Induced Self-Assembly (Photo-PISA): New Insights and Opportunities. *Adv. Sci.* **2017**, *4* (7), 1700137.

(5) Zhang, W.-J.; Hong, C.-Y.; Pan, C.-Y. Polymerization-Induced Self-Assembly of Functionalized Block Copolymer Nanoparticles and Their Application in Drug Delivery. *Macromol. Rapid Commun.* **2019**, *40* (2), 1800279.

(6) D'Agosto, F.; Rieger, J.; Lansalot, M. RAFT-Mediated Polymerization-Induced Self-Assembly. *Angew. Chem., Int. Ed.* **2020**, *59* (22), 8368−8392.

(7) Derry, M. J.; Fielding, L. A.; Armes, S. P. Polymerization-Induced Self-Assembly of Block Copolymer Nanoparticles via RAFT Non-Aqueous Dispersion Polymerization. *Prog. Polym. Sci.* **2016**, *52*, 1−18.

(8) Wright, D. B.; Touve, M. A.; Adamiak, L.; Gianneschi, N. C. ROMPISA: Ring-Opening Metathesis Polymerization-Induced Self-Assembly. *ACS Macro Lett.* **2017**, *6* (9), 925−929.

(9) Khor, S. Y.; Quinn, J. F.; Whittaker, M. R.; Truong, N. P.; Davis, T. P. Controlling Nanomaterial Size and Shape for Biomedical Applications via Polymerization-Induced Self-Assembly. *Macromol. Rapid Commun.* **2019**, *40* (2), 1800438.

(10) Guégain, E.; Zhu, C.; Giovanardi, E.; Nicolas, J. Radical Ring-Opening Copolymerization-Induced Self-Assembly (RROPISA). *Macromolecules* **2019**, *52* (10), 3612−3624.

(11) Grazon, C.; Salas-Ambrosio, P.; Ibarboure, E.; Buol, A.; Garanger, E.; Grinstaff, M. W.; Lecommandoux, S.; Bonduelle, C. Aqueous Ring-Opening Polymerization-Induced Self-Assembly (ROPISA) of N-Carboxyanhydrides. *Angew. Chem., Int. Ed.* **2020**, *59* (2), 622−626.

(12) Liu, C.; Hong, C.-Y.; Pan, C.-Y. Polymerization Techniques in Polymerization-Induced Self-Assembly (PISA. *Polym. Chem.* **2020**, *11* (22), 3673−3689.

(13) Boott, C. E.; Gwyther, J.; Harniman, R. L.; Hayward, D. W.; Manners, I. Scalable and Uniform 1D Nanoparticles by Synchronous Polymerization, Crystallization and Self-Assembly. *Nat. Chem.* **2017**, *9*, 785.

(14) Sha, Y.; Rahman, M. A.; Zhu, T.; Cha, Y.; McAlister, C. W.; Tang, C. ROMPI-CDSA: Ring-Opening Metathesis Polymerization-Induced Crystallization-Driven Self-Assembly of Metallo-Block Copolymers. *Chem. Sci.* **2019**, *10* (42), 9782−9787.

(15) Hurst, P. J.; Rakowski, A. M.; Patterson, J. P. Ring-Opening Polymerization-Induced Crystallization-Driven Self-Assembly of Poly-L-Lactide-Block-Polyethylene Glycol Block Copolymers (ROPI-CDSA. *Nat. Commun.* **2020**, *11* (1), 4690.

(16) Peterson, I.; Yang, G.; Choi, S. T.-L. Direct Formation of Nano-Objects via in Situ Self-Assembly of Conjugated Polymers. *Polym. Chem.* **2021**, *12* (10), 1393−1403.

(17) Hwang, S.-H.; Kang, S.-Y.; Yang, S.; Lee, J.; Choi, T.-L. Synchronous Preparation of Length-Controllable 1D Nanoparticles via Crystallization-Driven In Situ Nanoparticlization of Conjugated Polymers. *J. Am. Chem. Soc.* **2022**, *144* (13), 5921−5929.
(18) Guan, S.; Chen, A. One-Pot Synthesis of Cross-Linked Block Copolymer Nanowires via Polymerization-Induced Hierarchical Self-Assembly and Photodimerization. *ACS Macro Lett.* **2020**, *9* (1), 14−19.
(19) Takahashi, R.; Miwa, S.; Sobotta, F. H.; Lee, J. H.; Fujii, S.; Ohta, N.; Brendel, J. C.; Sakurai, K. Unraveling the Kinetics of the Structural Development during Polymerization-Induced Self-Assembly: Decoupling the Polymerization and the Micelle Structure. *Polym. Chem.* **2020**, *11* (8), 1514−1524.
(20) Wang, J. Tuning Polymerization Rate Program Block Copolymer Assemblies in PISA: A Simulation Study. *IOP Conf. Ser. Mater. Sci. Eng.* **2020**, *859*, 012007.
(21) Wang, J.; Fang, T.; Li, J.; Yan, Y.; Li, Z.; Zhang, J. Precise Mesoscopic Model Providing Insights into Polymerization-Induced Self-Assembly. *Langmuir* **2020**, *36* (27), 8009−8016.
(22) Luo, X.; Zhao, S.; Chen, Y.; Zhang, L.; Tan, J. Switching between Thermal Initiation and Photoinitiation Redirects RAFT-Mediated Polymerization-Induced Self-Assembly. *Macromolecules* **2021**, *54* (6), 2948−2959.
(23) Blackman, L. D.; Doncom, K. E. B.; Gibson, M. I.; O'Reilly, R. K. Comparison of Photo- and Thermally Initiated Polymerization-Induced Self-Assembly: A Lack of End Group Fidelity Drives the Formation of Higher Order Morphologies. *Polym. Chem.* **2017**, *8* (18), 2860−2871.
(24) R. Guimarães, T.; Loong Bong, Y.; W. Thompson, S.; Moad, G.; Perrier, S.; B. Zetterlund, P. Polymerization-Induced Self-Assembly via RAFT in Emulsion: Effect of Z-Group on the Nucleation Step. *Polym. Chem.* **2021**, *12* (1), 122−133.
(25) Jones, E. R.; Semsarilar, M.; Wyman, P.; Boerakker, M.; Armes, S. P. Addition of Water to an Alcoholic RAFT PISA Formulation Leads to Faster Kinetics but Limits the Evolution of Copolymer Morphology. *Polym. Chem.* **2016**, *7* (4), 851−859.
(26) Dove, A. P. Organic Catalysis for Ring-Opening Polymerization. *ACS Macro Lett.* **2012**, *1* (12), 1409−1412.
(27) Kamber, N. E.; Jeong, W.; Waymouth, R. M.; Pratt, R. C.; Lohmeijer, B. G. G.; Hedrick, J. L. Organocatalytic Ring-Opening Polymerization. *Chem. Rev.* **2007**, *107* (12), 5813−5840.
(28) Pratt, R. C.; Lohmeijer, B. G.; Long, D. A.; Waymouth, R. M.; Hedrick, J. L. Triazabicyclodecene: A Simple Bifunctional Organocatalyst for Acyl Transfer and Ring-Opening Polymerization of Cyclic Esters. *J. Am. Chem. Soc.* **2006**, *128* (14), 4556−4557.
(29) Pratt, R. C.; Lohmeijer, B. G. G.; Long, D. A.; Lundberg, P. N. P.; Dove, A. P.; Li, H.; Wade, C. G.; Waymouth, R. M.; Hedrick, J. L. Exploration, Optimization, and Application of Supramolecular Thiourea−Amine Catalysts for the Synthesis of Lactide (Co)-Polymers. *Macromolecules* **2006**, *39* (23), 7863−7871.
(30) Lohmeijer, B. G. G.; Pratt, R. C.; Leibfarth, F.; Logan, J. W.; Long, D. A.; Dove, A. P.; Nederberg, F.; Choi, J.; Wade, C.; Waymouth, R. M.; Hedrick, J. L. Guanidine and Amidine Organocatalysts for Ring-Opening Polymerization of Cyclic Esters. *Macromolecules* **2006**, *39* (25), 8574−8583.
(31) Czajka, A.; Armes, S. P. In Situ SAXS Studies of a Prototypical RAFT Aqueous Dispersion Polymerization Formulation: Monitoring the Evolution in Copolymer Morphology during Polymerization-Induced Self-Assembly. *Chem. Sci.* **2020**, *11* (42), 11443−11454.
(32) Gyorgy, C.; Hunter, S. J.; Girou, C.; Derry, M. J.; Armes, S. P. Synthesis of Poly(Stearyl Methacrylate)-Poly(2-Hydroxypropyl Methacrylate) Diblock Copolymer Nanoparticles via RAFT Dispersion Polymerization of 2-Hydroxypropyl Methacrylate in Mineral Oil. *Polym. Chem.* **2020**, *11* (28), 4579−4590.
(33) Ilday, S.; Makey, G.; Akguc, G. B.; Yavuz, Ö.; Tokel, O.; Pavlov, I.; Gülseren, O.; Ilday, F. Ö. Rich Complex Behaviour of Self-Assembled Nanoparticles Far from Equilibrium. *Nat. Commun.* **2017**, *8* (1), 14942.
(34) Szavits-Nossan, J.; Eden, K.; Morris, R. J.; MacPhee, C. E.; Evans, M. R.; Allen, R. J. Inherent Variability in the Kinetics of Autocatalytic Protein Self-Assembly. *Phys. Rev. Lett.* **2014**, *113* (9), 098101.
(35) Dighe, A. V.; Huelsenbeck, L.; Bhawnani, R. R.; Verma, P.; Stone, K. H.; Singh, M. R.; Giri, G. Autocatalysis and Oriented Attachment Direct the Synthesis of a Metal−Organic Framework. *JACS Au* **2022**, *2* (2), 453−462.
(36) Shen, L.; Bu, H.; Yang, H.; Liu, W.; Li, G. Investigation on the Behavior of Collagen Self-Assembly in Vitro via Adding Sodium Silicate. *Int. J. Biol. Macromol.* **2018**, *115*, 635−642.
(37) McQuade, D. T.; McKay, S. L.; Powell, D. R.; Gellman, S. H. Indifference to Hydrogen Bonding in a Family of Secondary Amides. *J. Am. Chem. Soc.* **1997**, *119* (36), 8528−8532.
(38) Rizvi, A.; Mulvey, J. T.; Carpenter, B. P.; Talosig, R.; Patterson, J. P. A Close Look at Molecular Self-Assembly with the Transmission Electron Microscope. *Chem. Rev.* **2021**, *121* (22), 14232−14280.
(39) Inam, M.; Cambridge, G.; Pitto-Barry, A.; Laker, Z. P. L.; Wilson, N. R.; Mathers, R. T.; Dove, A. P.; O'Reilly, R. K. 1D vs. 2D Shape Selectivity in the Crystallization-Driven Self-Assembly of Polylactide Block Copolymers. *Chem. Sci.* **2017**, *8* (6), 4223−4230.
(40) He, X.; He, Y.; Hsiao, M.-S.; Harniman, R. L.; Pearce, S.; Winnik, M. A.; Manners, I. Complex and Hierarchical 2D Assemblies via Crystallization-Driven Self-Assembly of Poly(l-Lactide) Homopolymers with Charged Termini. *J. Am. Chem. Soc.* **2017**, *139* (27), 9221−9228.
(41) Parent, L. R.; Bakalis, E.; Ramírez-Hernández, A.; Kammeyer, J. K.; Park, C.; de Pablo, J.; Zerbetto, F.; Patterson, J. P.; Gianneschi, N. C. Directly Observing Micelle Fusion and Growth in Solution by Liquid-Cell Transmission Electron Microscopy. *J. Am. Chem. Soc.* **2017**, *139* (47), 17140−17151.

https://doi.org/10.1021/acspolymersau.2c00027
ACS Polym. Au 2022, 2, 501−509